Reprint from

Andrey L. Rogach (ed.)
Semiconductor Nanocrystal Quantum Dots
Synthesis, Assembly, Spectroscopy and Applications

Anti-Stokes photoluminescence in semiconductor nanocrystal quantum dots

By

Yury P. Rakovich, John F. Donegan

School of Physics and CRANN Research Centre, Trinity College Dublin, Dublin, Ireland

1. Introduction

George Gabriel Stokes, while studying the process of light emission from solid materials, discovered that the wavelength of the emitted light is generally longer than that of the light which is exciting the emission process. This excitation–emission shift bears his name, as an observed "Stokes-shift" between the excited and emitted light [1]. In our modern quantum mechanical description of the process, the emitted photons have a lower energy than those exciting the photoluminescence, the excess energy being delivered into the material, usually by phonon excitation. Within this review, we call the process the Stokes-shifted photoluminescence (SSPL).

It has been shown that some materials emit light at shorter wavelengths than that with which the material was illuminated because of thermal (phonon) interactions with the excited atoms [2]. This up-conversion process is termed anti-Stokes photoluminescence (ASPL), as opposed to the more common Stokes emission process. ASPL has been observed in a variety of systems such as atoms and molecules [3, 4], polymers [5, 6], fullerenes [7, 8], semiconductor macrocrystals [9–14] and structures [15–23].

Recent research interest in the field of up-conversion processes has been sparked by the development of multi-colour displays [24], dynamical imaging microscopy [25], bio-imaging systems [26, 27], unconventional lasers [28] and solid-state optical refrigeration devices [29, 30]. Here, we will concentrate on one particular up-conversion process, phonon-assisted anti-Stokes emission, in one particular type of semiconductor nanostructures, namely in nanocrystal quantum dots (QDs) fabricated via colloidal chemistry. These QDs represent the ultimate in semiconductor-based quantum-confined systems with atom-like energy levels, large optical transition dipole moment and high photoluminescence (PL) quantum efficiency. The interest developed in nanocrystal QDs has been fueled by the high degree of reproducibility and control that is currently available in the fabrication and manipulation of these quantum-confined structures [31]. It is worth mentioning the utilization of QDs in LEDs [32, 33], photonic [34, 35] and core-shell structures [36, 37], and as biological labels [38, 39].

Apart from phonon-assisted up-conversion [40] a number of different mechanisms have been suggested to explain the anti-Stokes emission process. The suggested microscopic mechanisms are Auger recombination [15, 41], direct two-photon absorption [42, 43], and two-step/two-photon absorption [44]. Below, we will discuss the plausibility of these mechanisms in the ASPL of semiconductor nanocrystals.

2. Phonon-assisted ASPL in nanocrystal QDs

The ASPL occurs when the emission spectrum with intensity I_{em} is obtained at higher energy than the excitation (P) (Fig. 1) while the energy gap ΔE between the excitation energy and the excited electronic level is comparable or even large than the maximum phonon energy in the material. It is instructive to start the consideration of the problem with a simple three-level model where two upper energy levels are separated by an energy gap of value ΔE (Fig. 1a).

To set up rate equations, we first consider the excitation transition from the ground state ("0") to the state "1", from where two pathways are possible. First, the resonant radiative transition from state "1" may return the system to its ground state with rate γ_1. Alternatively, a thermally induced population of level "2" may occur with a radiative transition, which is the ASPL process, from state "2" with rate γ_2. At elevated temperatures this process may prevail over the resonant recombination. The excited carriers may relax nonradiatively from level "2" to level "1" with rate γ_r followed by the resonant radiative recombination.

The dynamic equations, which describe this model for population densities n_1 and n_2 are

$$\begin{aligned} \frac{dn_1}{dt} &= P - [\gamma_1 + \gamma_r \exp(-\Delta E/kT)]n_1 + \gamma_r n_2 \\ \frac{dn_2}{dt} &= \gamma_r \exp(-\Delta E/kT)n_1 - \gamma_r n_2 - \gamma_2 n_2 \end{aligned} \tag{1}$$

where γ_i is the recombination rate; ΔE is the activation energy; k is Boltzmann's constant; T is the temperature.

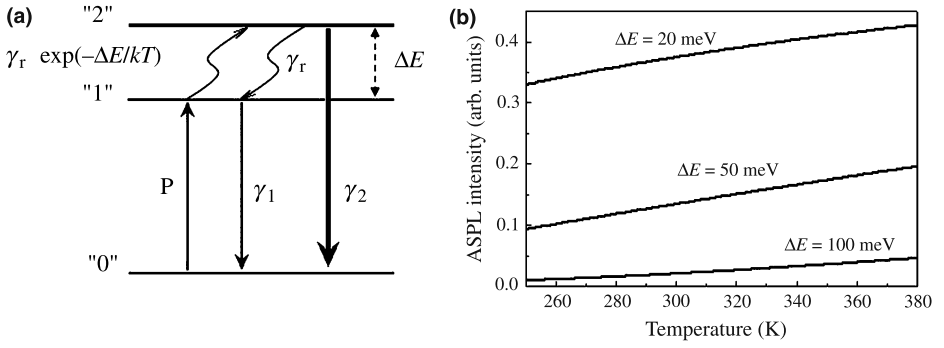

Fig. 1. Energy scheme for phonon-assisted up-converted emission (**a**) and temperature dependence of ASPL intensity calculated using Eq. (2) for three values of ΔE supposing that $\gamma_r = \gamma_1 = \gamma_2$ (**b**)

Solving system (1) for continuous-wave excitation one obtains equations for both the resonant emission ($I_1 = \gamma_1 n_1$) and up-converted emission intensity ($I_2 = \gamma_2 n_2$):

$$I_1 = P\frac{c_1}{c_1 + A\exp(-\Delta E/kT)}$$
$$I_2 = P\frac{A\exp(-\Delta E/kT)}{c_2 + A\exp(-\Delta E/kT)} \quad (2)$$

where coefficients $c_1 = \gamma_1/\gamma_r$; $c_2 = \gamma_2/\gamma_r$; $A = \gamma_2/(\gamma_2 + \gamma_r)$ describe the ratios of recombination rates. It is noteworthy that experimentally these parameters can be estimated from analysis of the PL decay curve [31, 45].

The first implication of this analysis is that the intensity of up-converted emission is a linear function of excitation power. However, the most striking feature of this model is that the intensity of the up-converted emission increases with temperature (Fig. 1b) gaining energy from the thermal bath in contrast to the conventional quenching of resonant or Stokes-shifted luminescence with increasing temperature. This anomalous temperature behaviour of ASPL may therefore be used as an indicator of phonon-assisted processes while analysing mechanisms of up-converted luminescence in materials.

To date ASPL caused by one-photon phonon-assisted carrier excitation has been reported for InP [46], CdSe [46–48], CdTe [47, 49, 50], PbS [51] and PbSe [52] nanocrystals.

3. Dependence on excitation wavelength and the efficiency of ASPL

A general feature of this kind of up-conversion process is that the ASPL signal can be detected only for excitation energies that are well below the maximum energy position of the normal Stokes emitted PL signal.

Figure 2a shows PL spectra of 4-nm size CdSe/ZnS QDs measured at room temperature varying the excitation energy (E_{exc}) (2.0–3.10 eV) in the spectral region from the high energy region of the absorption spectra to the tail far below the first absorption peak (Fig. 2b). When $E_{exc} = 2.43$ eV (Fig. 2a, Region I) the position of the Stokes-shifted emission peak is almost independent of the excitation wavelength. For this sample, the value of the "nonresonant Stokes shift" (the difference between the lowest-energy peak in the absorption spectra and the emission peak) is about 67 meV. The PL linewidth shows only a very small additional broadening with increasing excitation energy in this region. This weak dependence of the linewidth and the nonresonant Stokes shift is due to the fact that the higher the excitation energy – the better the PL spectrum reflects the entire size distribution of nanocrystals in the sample. While the data presented in Fig. 2a are normalized for comparison, on an absolute scale, a 57% reduction in the integrated PL intensity has been observed as the excitation energy decreases from 3.10 eV to 2.43 eV.

Providing excitation between 2.30 and 2.43 (Fig. 2a, Region II), the emission profile becomes more complex. A weak shoulder appears on the blue edge of PL band as the photon energy decreases down to 2.38 eV, whereas the main PL peak shifts to the low-energy side. For lower energy excitation (2.34 eV), the PL spectrum has one

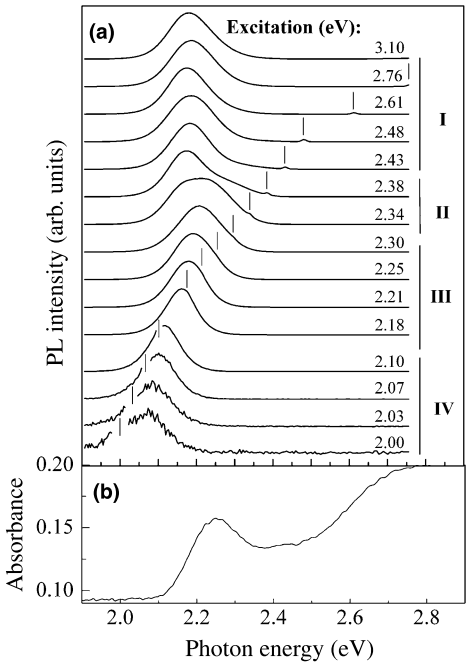

Fig. 2. **a** PL spectra of CdSe/ZnS nanocrystals in toluene for various excitation wavelengths at room temperature. For each spectrum the excitation energy is marked by a vertical line. All PL spectra are normalized for comparison. **b** The absorption spectrum of the sample

very broad band, which can be well de-convoluted into two peaks. This double peak structure can be explained as a result of size-selective excitation within the population of QDs and is expected for an inhomogeneously broadened system. Since there are multiple states present, there is a photon energy (2.38–2.34 eV) where the largest QDs can be excited into their second excited state, while a smaller size is excited into their first excited state. Since each nanocrystal emits at one photon energy, regardless of excitation energy, at this point the emission spectrum shows two peaks, one from the smaller set of particles absorbing into their first state and the second from the larger QDs excited into their second state [53].

As the excitation photon energy is tuned further below the first absorption maximum of 2.25 eV down to 2.18 eV (Fig. 2a, Region III), one PL peak is observed again, whose emission energy shifts to the red with decreasing excitation energy. The width of the PL peak decreases considerably in this spectral region (from ~137 meV at $E_{exc} = 2.30$ eV to ~96 meV at $E_{exc} = 2.18$ eV) demonstrating PL line narrowing, because only larger nanocrystals within the finite size distribution are excited on the low-energy side of the absorption profile. On the other hand, a 52% reduction in the integrated PL intensity has been observed as the excitation energy decreases in Region II because only a very small fraction of the size distribution is selected to be excited.

A distinctly different behaviour is observed in the spectral region far below the absorption peak (Fig. 2a, Region IV). A tail of ASPL can be seen with 2.10 eV

excitation, ranging up to ~200 meV above the excitation energy. A similar decaying anti-Stokes tail in PL has been also observed in InP [46] and CdTe nanocrystals [54]. At still lower excitation energies, a pronounced ASPL peak appears in the high-energy region, which shifts to lower energy following the excitation wavelength. This behaviour is very similar to that of the SSPL in region III. Actually, the progressive transition from SSPL into ASPL is evident in Fig. 2a, Regions III–IV. A similar observation was reported recently for PbS QDs [51]. The gradual change in the band shape suggests that the physical process involved in QD emission is the same throughout the whole range of excitation energies. However, in contrast to SSPL, the ASPL does not reflect the size distribution of the QDs. As mentioned above, the effect of inhomogeneous broadening caused by the distribution of QDs sizes can be clearly seen in the excitation wavelength dependence of the SSPL spectra (Fig. 2a, Regions II and III). When the excitation is restricted to the onset region of the absorption spectra, then QDs of a much narrower size range are excited; these QDs are the largest size in the ensemble. In this spectral region the SSPL spectra of QDs show a decrease of the width of the PL band demonstrating pronounced line narrowing [53, 55, 56]. In the spectra presented in Fig. 2a, the full width at half maximum (FWHM) of the SSPL band decreased from 95 meV at $E_{ex} = 2.32$ eV to 76 meV at $E_{ex} = 2.16$ eV. In contrast, the ASPL linewidth shows extra broadening with decreasing excitation energy: from 83 meV at $E_{ex} = 2.12$ eV to 150 meV at $E_{ex} = 1.95$ eV.

It is noteworthy that all spectra presented in Fig. 2a were obtained by exciting the samples with a Xenon lamp (output power of 40 μW to 0.1 mW, depending on the spectral region). This demonstrates that phonon-assisted excitation of the ASPL process in QDs is a highly efficient process since even for samples with moderate quantum yield (~20%) there is no need for laser excitation [57]. Also it can be seen that the efficiency of ASPL is comparable with that of SSPL at least for small magnitudes of the up-converted blue shift ΔE (at excitation energy $E_{ex} = 2.10$ eV). At lower excitation energies (i.e. bigger magnitudes of ΔE) the efficiency of ASPL rapidly declines in accordance with Vavilov's law [50, 58].

4. Dependence on excitation power

In light of the above model for population densities, photon energy up-conversion is a linear process of the excitation intensity in nanocrystal QDs. The linear behaviour of the ASPL intensity (I_{ASPL}) has been experimentally verified for various QD materials [46, 47, 49, 50, 59] with a slope depending on the quantum yield of the sample (Fig. 3).

It is known [46, 60] that in some cases, the analysis of the dependence of the ASPL intensity on the excitation intensity (I_{exc}) can give information on the mechanism of excitation energy transfer in the high-energy spectral region. Thus, with two-photon excitation or two-stage excitation of electrons from the valence to the conduction band through deep impurity levels, a quadratic dependence $I_{ASPL} \sim {I_{exc}}^2$ should be observed [60]. For an ASPL process induced by Auger recombination, the dependence $I_{ASPL} \sim {I_{exc}}^3$ is characteristic [22], whereas in the case of mixed mechanisms, the power-law dependence of I_{ASPL} on I_{exc} becomes more complicated [13].

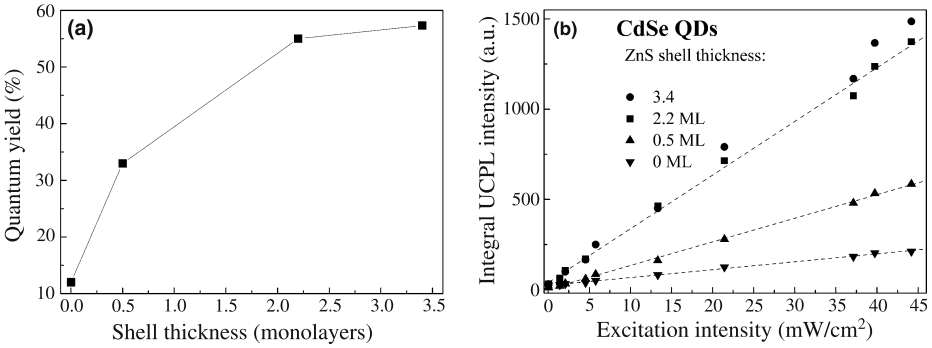

Fig. 3. **a** The PL quantum yield of CdSe QDs as a function of the ZnS shell thickness (in monolayers (ML)). The dashed line is a guide to the eye. **b** The dependence of the ASPL intensity in CdSe QDs on the excitation power density at room temperature. The lines show a linear fit to the data. The enhancement of up-conversion efficiency is observed with increasing of thickness of the ZnS shell, i.e. with improving passivation of surface dangling bonds. Reproduced with permission from MAIK Nauka/ Interperiodica [48]

Therefore, when analyzing an up-converted PL signal, an observed linear dependence of ASPL on excitation intensity alone cannot be taken as an indication of the participation of phonons in the excitation process. As will be discussed in the following section, the same dependence can be observed, for example, for two-photon or two-step excitation under conditions of saturation [61]. A definitive conclusion for the mechanisms of ASPL must be supported by a series of independent measurements. In this respect the temperature dependence investigations of up-converted PL are the most conclusive [46, 47, 49, 61, 62].

5. Temperature dependence of ASPL

As mentioned above, the ASPL process with a linear dependence on excitation intensity can be observed as a result of energy transfer to the excited electron–hole pair from the phonon bath. In this case, the ASPL intensity should grow with increasing temperature because of the increase of the population of phonons. Indeed, this behavior was reported for CdSe [46, 47] and CdTe [47, 49, 50] QDs. As can be seen from Fig. 4 an increase of up to 12 times in the ASPL intensity of CdSe QDs was achieved, when the sample was heated in the temperature range 283–353 K, while the width of ASPL band is gradually reduced [63]. At the same time the SSPL shows thermal induced quenching and broadening. It turns out that the thermally stimulated increase in the ASPL is almost independent of the size of the QDs (Fig. 5, inset), although it is more efficient when the QD surface is better passivated (Fig. 4, inset) [48, 49, 57].

The spectral position of the ASPL peak shows little dependence on temperature (Figs. 4 and 5) whereas the temperature variation of the peak energy of the SSPL was found to be practically coincident with that of the ($1S_e \rightarrow 1S_{3/2}$) absorption peak energy. These experimental findings demonstrate an important role of the electron–phonon interaction in ASPL processes in QDs and this will be considered later.

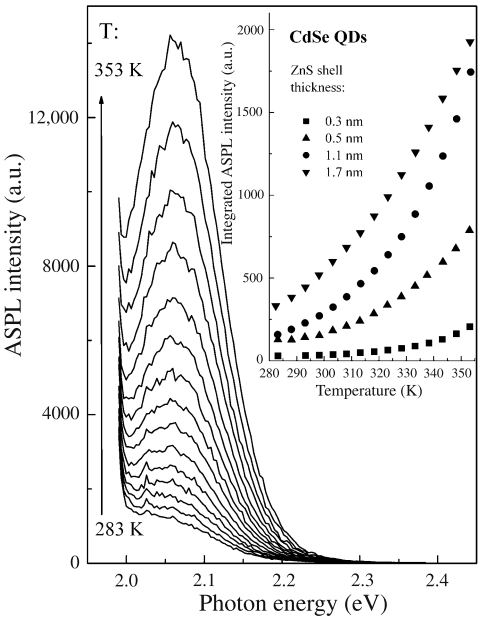

Fig. 4. Temperature dependence of the ASPL in 4-nm CdSe QDs with 1.1-nm ZnSe shell. Inset: Temperature stimulated enhancement of ASPL intensity for increasing shell thickness (i.e. increasing quantum yield of the sample). Reproduced with permission from MAIK Nauka/Interperiodica [48]

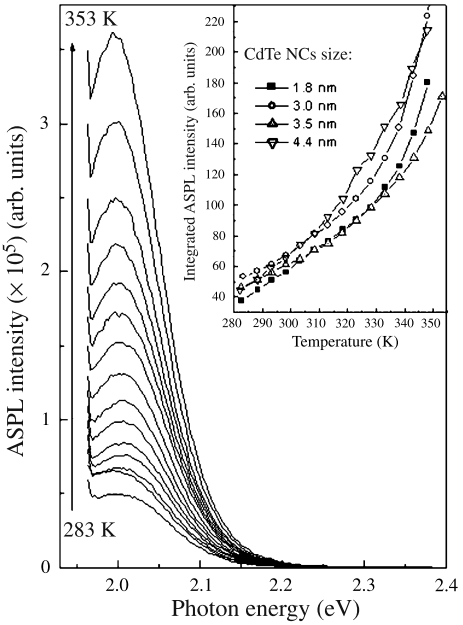

Fig. 5. Temperature behaviour of the ASPL band in 3.5-nm CdTe NCs. Inset: Variation of the integrated intensity of the ASPL with temperature for all samples studied. Reproduced with permission from Materials Research Society [57]

Table 1. The maximum magnitude of the anti-Stokes shift for different QD materials

Material	ΔE^{max} (meV)	References
CdSe	335	[47]
	413	[59]
CdTe	285	[47]
	350	[57]
	360	[49]
PbS	330	[51]

As can be seen from Fig. 1b, an increase in ASPL intensity with temperature strongly depends on the magnitude of the up-converted blue shift demonstrating a sub-linear growth at small (20 meV) values of ΔE; almost linear dependence is obtained for $\Delta E = 50$ meV and a super-linear exponential-like dependence for $\Delta E = 100$ meV.

For a phonon-assisted mechanism, the minimum magnitude of the up-converted blue shift is expected to be about the typical energy of optical phonons (24.8 meV for the bulk CdSe) [64] which is comparable to the thermal energy ($\sim k_B T$) at room temperature. In data presented in Fig. 4, ΔE is about 97 meV giving rise to a well-resolved ASPL band.

As can be seen from Fig. 2, the value of the anti-Stokes blue shift increases with decreasing excitation energy. The maximum magnitude of the up-converted shift (ΔE^{max}) can be defined as the difference between the excitation energy and the energy value at which an exponential fit of the ASPL high-energy wing crosses the average background noise level [46]. The reported values of ΔE^{max} estimated in this way are summarized in Table 1.

6. Mechanism of ASPL: thermally populated defect states versus electron–phonon interaction

Let us summarize the reported experimental results on the ASPL in colloidal QDs:

(i) The ASPL intensity increases linearly with excitation power.

(ii) The ASPL intensity grows strongly with increasing temperature. The efficiency of the thermally stimulated ASPL growth is independent of the size of the QDs. The up-conversion process is more efficient in samples with higher quantum yield.

(iii) If E_{ex} increases (approaching the absorption peak) the ASPL peak moves continuously towards higher energy accompanied by a narrowing of the ASPL band. Its efficiency increases approaching the efficiency of SSPL and finally the spectrum switches to the Stokes-shifted regime.

(iv) The blue (anti-Stokes) shift between the ASPL peak and E_{ex} does not depend significantly upon QDs size. The shift can range approximately from 20 meV to 400 meV.

Possible ASPL mechanisms were discussed in [46–50, 57], but no definite conclusions were made. According to point (i) above, nonlinear optical processes such

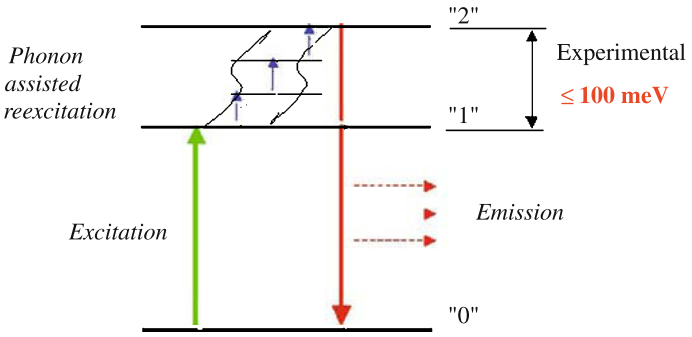

Fig. 6. Schematic of phonon-assisted up-conversion mechanism proposed in [47]

as two-photon absorption and (since the possibility of emergence of more than one-exciton per QD is negligible) the Auger excitation can be excluded in this case. Experimental findings (ii) and (iii) strongly suggest the involvement of phonons in the re-excitation process. Finally, in order to explain (iv), it was suggested that up-conversion occurs via thermally populated states. This mechanism requires that the defect states are populated via phonons and then absorption of the incident photon leads to the excitation into the conduction band states followed by the higher energy photon emission. Depending on the electronic structure of the conduction and valence energy levels in particular QDs, electron [47, 49] or hole [46] up-conversion is believed to be driven by phonon absorption.

Although theoretical data reported in support of this mechanism are consistent with the surface energy levels for dangling bonds or other sub-bandgap defect states, there is no direct experimental evidence that these states are responsible for the ASPL process [46, 49, 59]. Also the fact that the ASPL efficiency increases with quantum yield of the QDs provides strong proof that the ASPL emission cannot originate from sub-band gap states.

In order to account for all the experimental features of ASPL, an alternative model has been recently suggested based on direct re-excitation of QDs by longitudinal optical (LO) phonons without resorting to the surface (defect) states [65]. Taking advantage of a nonperturbative approach for the calculation of the polaronic effects in QDs, it was shown that red-shifted optical phonon replicas can be involved in up-conversion and that the polaronic effects are significant, even when the interlevel spacing in the QDs is quite far away from resonance with the optical phonon energies.

Figure 7a presents the lower-energy side of absorption spectrum of CdSe QDs calculated using this approach and showing two sub-bandgap bands (indicated as "−1LO" and "−2LO") through which the QDs can be excited. The QDs will then emit a photon most likely having the energy of the zero phonon line. In a sense 1LO and 2LO optical phonon replicas represent virtual sub-gap states, which are separated from the fundamental absorption line (i.e. zero phonon line) by energies that are only weakly dependent on the QD size. The probability of such an up-conversion process increases with temperature because so does the integrated intensity of the "−1LO" and "−2LO" absorption bands due to increased population of LO phonons (Fig. 7b). The experimental temperature dependence of the ASPL

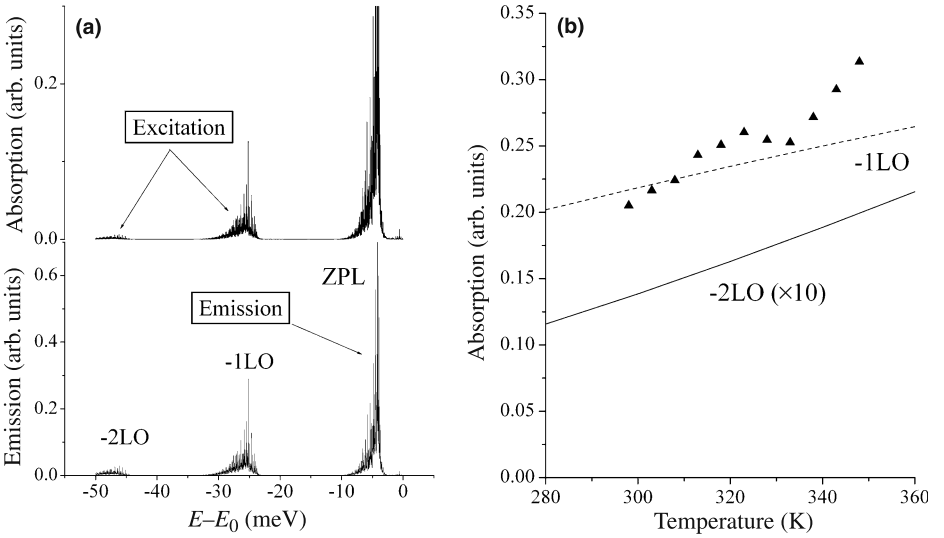

Fig. 7. **a** Low-energy part of the absorption and emission spectra calculated for a hypothetical CdTe QD considering three optical phonon modes with parameters given in the figure. The level spacing $\Delta E = 100$ meV, and the temperature is 300 K. **b** Temperature dependence of the integrated intensity of two sub-bandgap bands in the absorption spectrum (**a**) (lines) and experimental data of [47] (points) showing the temperature dependence of the ASPL peak amplitude. Reproduced with permission from American Physical Society [65]

intensity described above can be understood by taking into account that, at a certain temperature, further (higher order) red-shifted satellites (whose intensity depends more strongly on temperature) become more efficient.

In reality the situation is complicated by the distribution of the QD size, so that E_{ex} can match different "$-n$LO" bands of QDs of several different size subsets within the ensemble. It is also necessary to bear in mind that inter-level interaction, multiple confined optical phonon modes, and interaction with acoustic phonons will broaden the satellite band for each QDs in the ensemble. Consequently, the resulting ASPL band will not appear as a sum of narrow features as it appears from the above figure. Another complication arises from the fact that the calculated emission spectrum (Fig. 7a) assumes thermal equilibrium. This will be the case only if carrier thermalization processes are fast. Recent studies of carriers dynamics in QDs [55, 66, 67] at above bandgap excitation show that immediately after photoexcitation, the initially formed hot carriers thermalize quickly to the bottom of the conduction and valence bands and subsequently decay either into shallow trap states [55, 66] or an intrinsic "dark" exciton state [68]. This thermalization is an extremely fast process occurring in the 300–500 fs range [67, 69] providing fast establishment of thermal equilibrium. It is noteworthy that the reported time-resolved studies of ASPL demonstrate a much longer, ns-scale decay [49]. However, there is no reason why such relaxation should be slower at room temperature and/or if the carrier is "cool".

Another and more serious problem with the proposed polaronic mechanism of up-conversion is that using this approach it is difficult to explain the observed values of the up-converted shift (Table 1) which are much larger than the LO phonon energy.

Of course in spectra of individual QDs there are further "$-n$LO" satellites (with larger n), but their intensities are very low for realistic values of the electron–phonon coupling constants. In order to explain the experimentally observed large anti-Stokes shifts, one has to consider a cascaded mechanism of the ASPL. More detailed discussion of this particular mechanism is given in the chapter of M. Vasilevskiy of this book.

7. Availability of phonon modes

Whichever model is used to describe the phonon-assisted ASPL excitation in the QDs, the availability of vibrational modes is crucial to provide efficient up-conversion. To this end, recent experimental studies of Raman spectra in semiconductor QDs [70–75] may provide fresh insight into understanding the mechanism of phonon-assisted up-conversion.

The evolution of the optical phonon spectra of colloidal core/shell CdSe/ZnS QDs which demonstrate efficient ASPL (Figs. 2 and 4) has been recently reported [70]. These QDs were studied by resonant Raman spectroscopy with an increase of the shell thickness from 0.5 to 3.4 monolayers. A significant improvement of the PL efficiency has been observed with increase of the ZnS shell thickness.

As an example of the Raman spectra of the CdSe/ZnS nanocrystals, the spectrum of CdSe QDs with the thickest (3.4 ML) ZnS shell is presented in Fig. 8a. Raman lines of the LO and 2LO phonons of the CdSe core are clearly seen in the region of

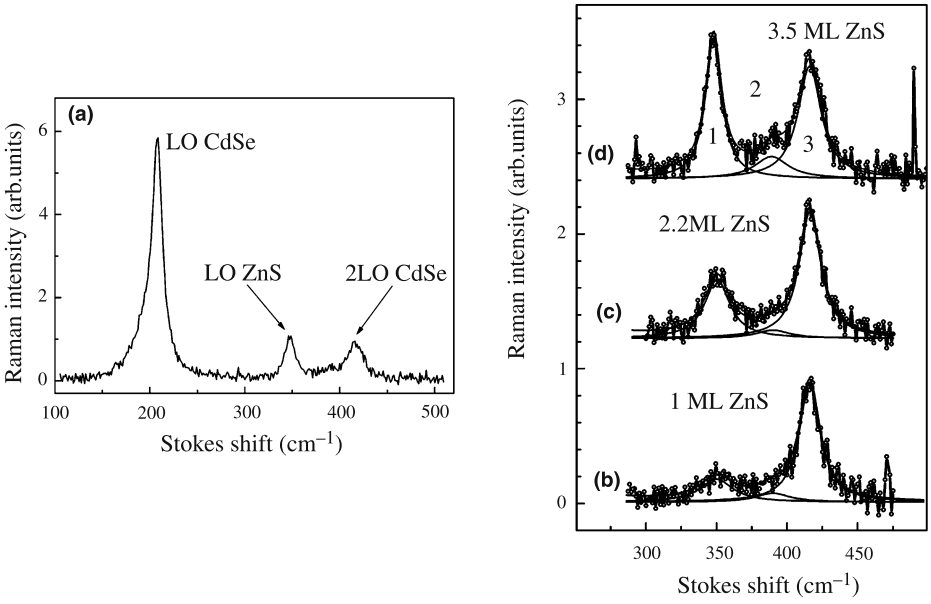

Fig. 8. **a** Raman spectrum of CdSe/ZnS QDs with a shell thickness 3.4 ML. **b–d** The parts of the Raman spectra of CdSe/ZnS QDs in the region of the ZnS LO phonon for different shell thicknesses. The regions of the ZnS LO phonons and 2SO and 2LO phonons of CdSe are denoted by the numbers 1, 2, and 3, respectively. Reproduced with permission from American Physical Society [70]

200 cm^{-1} and 400 cm^{-1}, respectively. Apart from these modes a pronounced peak associated with the LO phonons of the ZnS shell can be seen in Fig. 8a at about 350 cm^{-1}. The intensity and line shape of the ZnS LO line are determined by the shell crystallographic structure [70].

It has turned out that the ZnS LO phonon line at 350 cm^{-1}, which partly overlaps the second order Raman lines of the CdSe core, can be distinguished, even at a shell thickness of 0.5 ML. The increase in shell thickness results in the increase in the line intensity, which is roughly proportional to the ZnS volume. A remarkable decrease in linewidth from 30 cm^{-1} for the 0.5 ML shell down to 12.5 cm^{-1} for the 3.4 ML manifests to the substantial improvement in the shell crystallographic structure. It is particularly remarkable that the increase in the shell thickness results in an enhanced efficiency of the ASPL process (Figs. 3 and 4). The observed peak between the ZnS LO and CdSe 2LO phonon lines (Fig. 8) was the subject of extensive discussion in the last several years [72, 76–79]. In most of the studies it was suggested that the asymmetry in the low-frequency part of the LO phonon Raman peak of the CdSe QDs is caused mainly by surface optical (SO) phonon modes. In spite of the fact that the Raman scattering by the SO modes is forbidden for an ideal spherical shape of the QDs, the appearance of the SO peak in Raman spectra can be explained by the relaxation of the angular momentum phonon selection rule because of the lack of wave-vector conservation in QDs [78]. It has been also predicted that the SO mode can be observed in the Raman spectra in the case of a nonspherical shape of the QDs, as well as due to the effect of impurities or interface imperfections [72, 78].

The theory of Raman scattering by spherical particles predicts the participation of phonons with angular momenta $l = 0$, 1, 2 and 3 (0 and 2 through the Fröhlich mechanism while 1 and 3 through the optical deformation potential hole–phonon interaction). Normally only LO-type phonons are observed in the spectra of II–VI

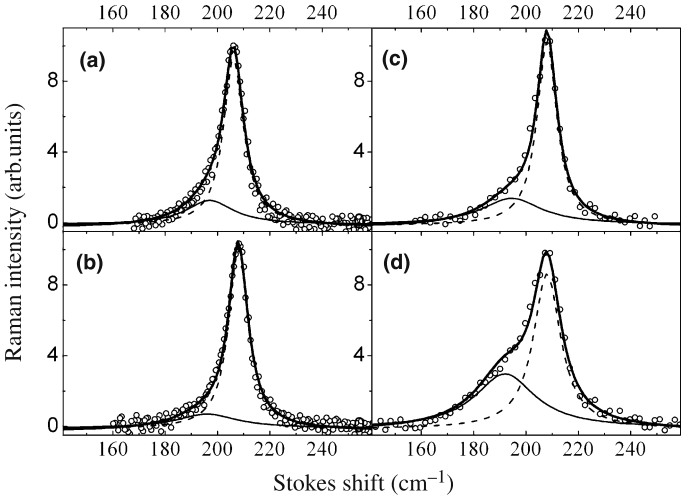

Fig. 9. The parts of the Raman spectra of CdSe/ZnS QDs in the region of the CdSe LO phonon for different shell thickness: 0 ML (**a**); 0.5 ML (**b**) 2.2 ML (**c**) and 3.4 ML (**d**), respectively. Reproduced with permission from American Physical Society [70]

QDs, and it was suggested that the polar Fröhlich-type interaction dominates the Raman scattering in CdSe/ZnS QDs. Therefore the peak labeled 2 in Fig. 8 can be assigned to the scattering from the interface phonon modes with $l = 2$ (although "breathing" $l = 0$ modes can also contribute to the polarised scattering).

A closer look at the evolution of the first order Raman spectra of the CdSe core as the ZnS shell thickness is varied reveals an enhanced contribution of SO modes (Fig. 9). The most striking result presented in Fig. 9 is the fact that with increasing shell thickness (i.e. with increase in quantum yield) the SO phonon band continues to shift to lower energy and grows in intensity. This was suggested to arise from an incoherent epitaxial growth of the ZnS shell at high coverage [70]. However, in the context of the present review, this fact clearly indicates the involvement of surface states in the up-conversion process, which is mediated by the interaction with optical surface phonons as well as with LO modes of the CdSe core and the ZnS shell. Due to spectral tunability of the SO mode energy (depending on shell thickness) optical phonon modes of various energies can contribute to the re-excitation of carriers causing efficient ASPL.

8. Applications of ASPL and further research directions

In the previous sections of this chapter, recent advances in the understanding of the fundamental properties of the phonon-assisted ASPL in semiconductor QDs are reviewed. In view of the potential applications, ASPL has a lot to offer in the fields of nanotechnology, lasing, optical cooling, bio-imaging and information technology. One of the applications suggested recently is the development of an all-optical temperature sensor based on nanoparticles [82]. Measurement of temperature changes in

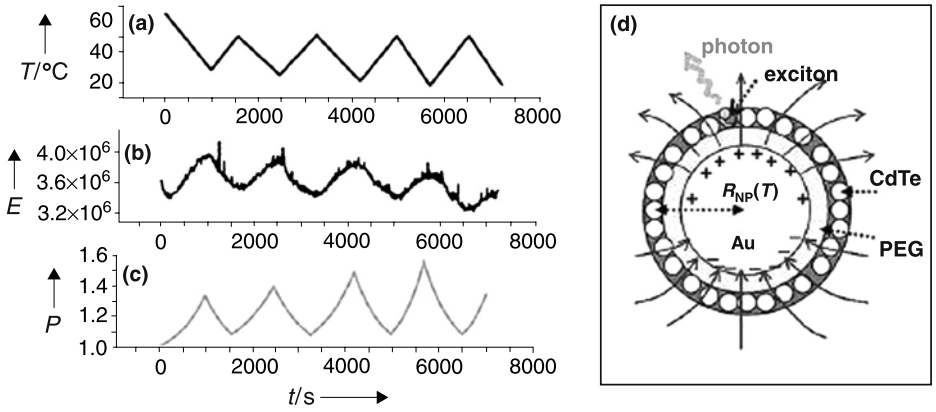

Fig. 10. Variation in the ASPL intensity E (**b**) of the PEG-tethered Au and CdTe QDs depending on the temperature T (**a**); **c** calculated photon-field enhancement factor P of the CdTe QDs as a function of time. **d** Schematic representation of the dielectric model used for calculating the curve in (**c**) as well as the plasmon excitation with associated field lines; the plasmon excitation inside an Au nanosphere interacts with excitons in the CdTe QDs through electric fields. The distance $R_{NP}(T)$ varies with the temperature. The curve in **c** also represents a theoretical dielectric model of the QDs assembly in which the CdTe QDs form a continuous spherical shell around the Au nanoparticles. Reproduced with permission from Wiley–VCH [82]

supersmall (nanoliter) volumes is a difficult problem, especially if both high precision and nanosecond time resolution are required.

One of the proposed approaches is to use the plasmon–exciton interaction in superstructures formed by metal nanoparticles and semiconductor QDs connected by a polymer acting as a molecular spring. A higher temperature leads to a modification in the luminescence due to the more extended conformation of the polymer chain (Fig. 10). In the reported experiments [82] the superstructure was excited in the anti-Stokes regime in order to eliminate scattered light from the excitation source.

Another promising direction is to use the unique properties of ASPL in hybrid photonic structures. In this respect whispering gallery mode (WGM) microcavities (e.g., microspheres, microcylinders, microrings and microtoroids) are ideally suited for observation of enhanced optical effects with extremely low excitation intensities [83]. High quality factors (Q) and large field densities associated with WGMs result in resonant enhancement of linear and nonlinear interactions of various kinds [36, 71, 84, 85]. Up-conversion of semiconductor QDs combined with photon confinement in three-dimensional microcavities has strong potential to be useful in micro-laser technology, optical data storage, lighting and bio-imaging applications.

Figure 11b shows a room temperature spectrum of a single polystyrene microsphere of 70 μm size covered by a monolayer of CdTe QDs on a Si substrate using low intensity nonresonance excitation by a He–Ne laser. The QD monolayer was formed

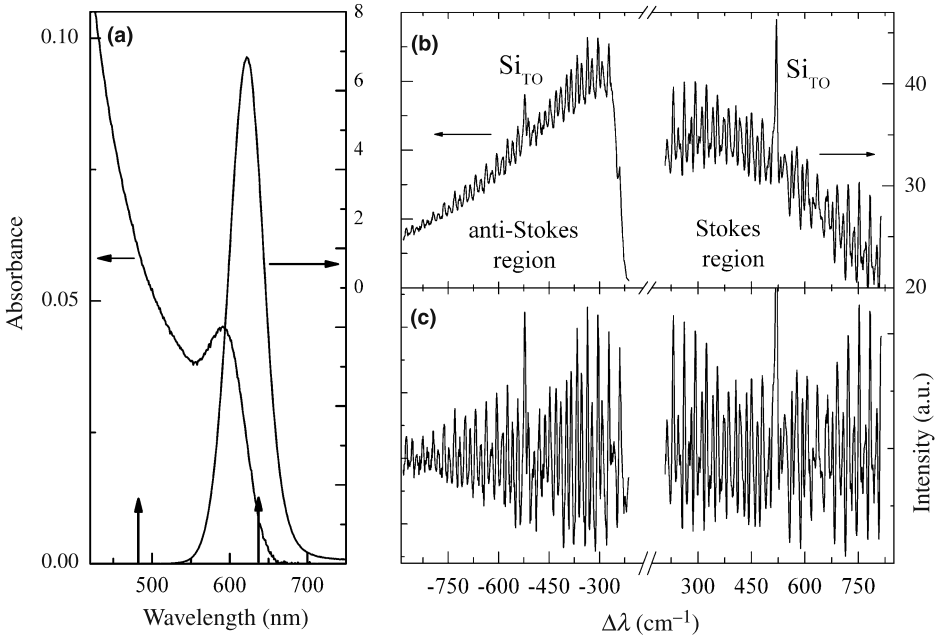

Fig. 11. Room temperature absorption and PL spectra of CdTe QDs in water (**a**). Arrows indicate the excitation wavelength used in micro-PL and Raman experiments. Raman spectrum of a single polystyrene/CdTe microsphere on a Si substrate. Excitation by HeNe laser $\lambda = 632.8$ nm before (**b**) and after (**c**) PL background subtraction. Reproduced with permission from Springer [86]

using the layer-by-layer deposition technique [37]. In this case, strong coupling between the WGM of the spherical microcavity and the electronic states of the CdTe QDs results in an enhanced luminescence contribution to the Raman signal simultaneously in both the Stokes and anti-Stokes spectral regions. The ASPL process is certainly highly efficient having an intensity comparable to the SSPL as seen from Fig. 11b. A similar effect was recently reported in small (2 μm) microspheres with a thin shell of semiconductor QDs [71]. The observation of ASPL from the polymer–CdTe microsphere can be attributed to the optical feedback via the microcavity with a WGM structure which leads to an increased probability of energy transfer to the emitting species.

A further major step in the application of ASPL using QDs is the development of nanoscale optical refrigerators. The concept of laser cooling (optical refrigeration) by luminescence up-conversion in solids dates back to 1929 [87], when it was recognized that thermal vibrational energy can be removed by anti-Stokes fluorescence creating a local cooling if a material is excited with photons having energy below the mean fluorescence energy. Material purity problems prevented observation of this type of laser cooling until 1995, when it was first demonstrated in ytterbium-doped glass [88]. This was followed soon after by reports of cooling in dye solutions [89] and thulium-doped glass [90]. A primary advantage of semiconductors compared to rare-earth doped solids is their potential for achieving temperatures down to $\sim$10 K and below [91]. This is due to the difference of the ground state populations in the two systems. Also colloidal semiconductor QDs have a number of advantages over dyes such as tunable absorption and emission wavelengths, better photostability and longer excited state lifetimes [92].

Although the theory of semiconductor cooling has been tackled previously [91, 93, 94], the critical issue hindering laser cooling applications is the limited quantum yield of semiconductor materials due to nonradiative carrier recombination. It was recently demonstrated that in order to achieve efficient optical cooling, the quantum yield must be higher than 90% [95] which is unachievable for bulk semiconductor materials or epitaxial heterolayers. However, recent advances in the synthesis of highly efficient colloidal QDs with suppressed nonradiative transitions [31] may allow for the realization of semiconductor cooling even below 10 K [91].

9. Conclusions

The unique optical properties of semiconductor colloidal QDs have enabled a comprehensive study of photon energy up-conversion mediated by the interaction with optical phonons. This has allowed for an improved understanding of the anti-Stokes luminescence in nanostructures. The study of phonon-assisted excitation of ASPL, reviewed here, reveals many fascinating questions and fundamental problems that appear when merging the main concepts of the electron–phonon interaction and electronic and photonic confinement, in one structure. The dependence of the ASPL parameters on the excitation intensity and temperature suggests a manifold of photonic applications, in particular in the fields of sensing and optical cooling.

Acknowledgements

We thank Prof. A. Eychmüller, Dr. N. Gaponik and Prof. M. I. Vasilevskiy for helpful discussions. This work was supported by Science Foundation Ireland (SFI) under its CRANN CSET Project PR23.

References

[1] Stokes GG (1858) On the change of refrangibility of light. Abstracts of the Papers Communicated to the Royal Society of London 6: 195–200
[2] Wood RW (1928) Anti-Stokes radiation of fluorescent liquids. Phil Mag 6: 310–315
[3] Shen YR (2003) The principles of nonlinear optics. Wiley-Interscience, Hoboken, NJ
[4] Pope M, Swenberg CE (1999) Electronic processes in organic crystals and polymers. Oxford University Press, Oxford
[5] Soos ZG, Kepler RG (1991) Two-photon-absorption spectrum of poly(di-n-hexylsilane) films. Phys Rev B 43: 11908–11912
[6] Lemmer U, Rischer R, Feldmann J, Mahrt RF, Yang J, Greiner A, Bassler H, Gobel EO, Heesel H, Kurz H (1993) Time-resolved studies of two-photon absorption processes in poly(p-phenylene-vinylene)s. Chem Phys Lett 203: 28–32
[7] Pichler K, Graham S, Gelsen OM, Friend RH, Romanow WJ, McCauley JP, Coustel N, Fischer JE, Smith AB (1991) Photophysical properties of solid films of fullerene, C_{60}. J Phys Condens Mater 3: 9259–9270
[8] Feldmann J, Fischer R, Guss W, Gobel EO, Schmitt-Rink S, Kratschmer W (1992) White luminescence from solid C_{60}. Europhys Lett 20: 553–558
[9] Litton CW, Reynolds DC, Collins TL, Park YS (1970) Exciton–LO-phonon interaction and anti-Stokes emission line in CdS. Phys Rev Lett 25: 1619–1621
[10] Halsted RE, Apple EF, Prener JS (1959) Two-State optical excitation in sulfide phosphors. Phys Rev Lett 2: 420–421
[11] Brown MR, Cox AFJ, Orr DS, Williams JM, Woods J (1970) Anti-Stokes excited edge emission in cadmium sulphide. J Phys C 3: 1767–1779
[12] Gundersen M (1974) Conversion of 28-mkm far-infrared radiation to visible light using bound excitons in CdS. Appl Phys Lett 24: 591–592
[13] Ivanov VY, Semenov YG, Surma M, Godlewski M (1996) Anti-Stokes luminescence in chromium-doped ZnSe. Phys Rev B 54: 4696–4701
[14] Ganichev D, Raab W, Zepezauer E, Prettl W, Yassievich IN (1997) Storage of electrons in shallow donor excited states of GaP:Te. Phys Rev B 55: 9243–9246
[15] Seidel W, Titkov A, Andre JP, Voisin P, Voos M (1994) High-efficiency energy up-conversion by an "Auger fountain" at an InP-AlInAs type-II heterojunction. Phys Rev Lett 73: 2356–2359
[16] Cho Y-H, Kim DS, Choe B-D, Lim H, Lee JL, Kim D (1997) Dynamics of anti-Stokes photoluminescence in type-II $Al_xGa_{1-x}As$ – $GaInP_2$ heterostructures: the important role of long-lived carriers near the surface. Phys Rev B 56: R4375–R4378
[17] Schrottke L, Grahn HT, Fujiwara K (1997) Enhanced anti-Stokes photoluminescence in a GaAs/$Al_{0.17}Ga_{0.83}As$ single quantum well with growth islands. Phys Rev B 56: R15553–R15556
[18] Finkeissen E, Potemski M, Wyder P, Vina L, Wiemann G (1999) Cooling of a semiconductor by luminescence up-conversion. Appl Phys Lett 75: 1258–1260
[19] Kral K, Zdenek P, Khas Z (2004) Transient processes and luminescence upconversion in zero-dimensional nanostructures. Surf Sci 566: 321–326
[20] Ignatiev IV, Kozin IE, Wen RN, Sugou S, Masumoto Y (1999) Anti-Stokes photoluminescence of InP self-assembled quantum dots in the presence of electric current. Phys Rev B 60: R14001–R14004
[21] Yamamoto A, Sasao T, Goto T, Arai K, Lee H-Y, Makino H, Yao T (2003) Anti-Stokes photoluminescence in CdSe self-assembled quantum dots. Phys Stat Sol (c) 0: 1246–1249
[22] Paskov PP, Holtz PO, Monemar B, Garcia JM, Schoenfeld WV, Petroff PM (2000) Photoluminescence up-conversion in InAs/GaAs self-assembled quantum dots. Appl Phys Lett 77: 812–814
[23] Kammerer C, Cassabois G, Voisin C, Delalande C, Roussignol P, Gerard JM (2001) Photoluminescence up-conversion in single self-assembled InAs/GaAs quantum dots. Phys Rev Lett 87: 207401–1/4
[24] Downing E, Hesselink L, Ralston J, Macfarlane R (1996) A three-color, solid-state, three-dimensional display. Science 273: 1185–1189
[25] Fujino T, Fujima T, Tahara T (2005) Femtosecond fluorescence dynamics imaging using a fluorescence up-conversion microscope. J Phys Chem B 109:15327–15331

[26] Kachynski AV, Kuzmin AN, Pudavar HE, Prasad PN (2005) Three-dimensional confocal thermal imaging using anti-Stokes luminescence. Appl Phys Lett 87: 023901–1/3
[27] Pena A-M, Strupler M, Boulesteix T, Schanne-Klein M-C (2005) Spectroscopic analysis of keratin endogenous signal for skin multiphoton microscopy. Opt Express 13: 6268–6274
[28] Macfarlane RM, Tong F, Silversmith AJ, Lenth W (1998) Violet cw neodymium upconversion laser. Appl Phys Lett 52: 1300–1302
[29] Luo X, Eisaman MD, Gosnell TR (1998) Laser cooling of a solid by 21 K starting from room temperature. Opt Lett 23: 639–641
[30] Thiede J, Distel J, Greenfield SR, Epstein RI (2005) Cooling to 208 K by optical refrigeration. Appl Phys Lett 86:154107–1/3
[31] Rogach AL, Franzl T, Klar TA, Feldmann J, Gaponik N, Lesnyak V, Shavel A, Eychmüller A, Rakovich YP, Donegan JF (2007) Aqueous synthesis of thiol-capped CdTe nanocrystals: state-of-the-art. J Phys Chem C 111: 14628–14637
[32] Colvin V, Schlamp M, Alivisatos A (1994) Light-emitting diodes made from cadmium selenide nanocrystals and a semiconducting polymer. Nature 370: 354–357
[33] Gao MY, Lesser C, Kirstein S, Mohwald H, Rogach AL, Weller H (2000) Electroluminescence of different colors from polycation/CdTe nanocrystal self-assembled films. J Appl Phys 87: 2297–2302
[34] Kershaw SV, Harrison MT, Burt MG (2003) Putting nanocrystals to work: from solutions to devices. Phil Trans 361: 331–343
[35] Rakovich YP, Donegan JF, Gerlach M, Bradley AL, Connolly TM, Boland JJ, Gaponik N, Rogach A (2004) Fine structure of coupled optical modes in photonic molecules. Phys Rev A 70: 051801 (R)–1/4
[36] Rakovich YP, Yang L, McCabe EM, Donegan JF, Perova T, Moore A, Gaponik N, Rogach A (2003) Whispering gallery mode emission from a composite system of CdTe nanocrystals and a spherical microcavity. Sem Sci Technol 18: 914–918
[37] Susha AS, Caruso F, Rogach AL, Sukhorukov GB, Kornowski A, Möhwald H, Giersig M, Eychmüller A, Weller H (2000) Formation of luminescent spherical core-shell particles by the consecutive adsorption of polyelectrolyte and CdTe(S) nanocrystals on latex colloids. Colloid Surf A 163: 39–44
[38] Alivisatos AP, Weiwei GW, Larabell C (2005) Quantum dots as cellular probes. Ann Rev Biomed Eng 7: 55–76
[39] Byrne SJ, Corr SA, Rakovich TY, Gun'ko YK, Rakovich YP, Donegan JF, Mitchell S, Volkov Y (2006) Optimisation of the synthesis and modification of CdTe quantum dots for enhanced live cell imaging. J Mater Chem 16: 2896–2902
[40] Auzel F (1976) Multiphonon-assisted anti-Stokes and Stokes fluorescence of triply ionized rare-earth ions. Phys Rev B 13: 2809–2817
[41] Potemski M, Stepniewski R, Maan JC, Martinez G, Wyder P, Etienne B (1991) Auger recombination within Landau levels in a two-dimensional electron gas. Phys Rev Lett 66: 2239–2242
[42] Cingolani R, Ploog K (1991) Frequency and density dependent radiative recombination processes in III-V semiconductor quantum-wells and superlattices. Adv Phys 40: 535–623
[43] Bhawalkar JD, Guang SH, Park C-K, Chan FZ, Ruland G, Prasad PN (1996) Efficient, two-photon pumped green upconverted cavity lasing in a new dye. Opt Commun 124: 33–37
[44] Baltramiejunas R, Vaitkus J, Gavryushin V (1978) Two-photon and two-step absorption of light in II–VI semiconductors. Sov Phys – Collection 18: 46–49
[45] Byrne SJ, Corr SA, Rakovich TY, Gun'ko YK, Rakovich YP, Donegan JF, Mitchell S, Volkov Y (2006) Optimisation of the synthesis and modification of CdTe quantum dots for enhanced live cell imaging. J Mater Chem 16: 2896–2902
[46] Poles E, Selmarten DC, Micic OI, Nozik AJ (1999) Anti-Stokes photoluminescence in colloidal semiconductor quantum dots. Appl Phys Lett 75: 971–973
[47] Rakovich YP, Filonovich SA, Gomes MJM, Donegan JF, Talapin DV, Rogach AL, Eychmüller A (2002) Anti-Stokes photoluminescence in II–VI colloidal nanocrystals. Phys Stat Sol (b) 229: 449–452
[48] Rusakov KI, Gladyshchuk AA, Rakovich YP, Donegan JF, Filonovich SA, Gomes MJM, Talapin DV, Rogach AL, Eychmüller A (2003) Control of efficiency of photon energy up conversion in CdSe/ZnS quantum dots. Opt Spectr 94: 921–925
[49] Wang X, Yu WW, Zhang J, Aldana J, Peng X, Xiao M (2003) Photoluminescence upconversion in colloidal CdTe quantum dots. Phys Rev B 68: 125318–1/6
[50] Rakovich YP, Gladyshchuk AA, Rusakov KI, Filonovich SA, Gomes MJM, Talapin DV, Rogach AL, Eychmüller A (2002) Anti-Stokes luminescence of cadmium telluride nanocrystals. J Appl Spectr 69: 444–449

[51] Fernee MJ, Jensen P, Rubinsztein-Dunlop H (2007) Unconventional photoluminescence upconversion from PbS quantum dots. Appl Phys Lett 91: 043112–1/3
[52] Harbold JM, Wise FW (2007) Photoluminescence spectroscopy of PbSe nanocrystals. Phys Rev B 76: 125304–125306
[53] Hoheisel W, Colvin VL, Johnson CS, Alivisatos AP (1994) Thereshold for quasicontinuum absorption and reduced luminescence efficiency in CdSe nanocrystals. J Chem Phys 101: 8455– 8460
[54] Talapin DV, Haubold S, Rogach AL, Kornowski A, Haase M, Weller H (2001) A novel organometallic synthesis of highly luminescent CdTe nanocrystals. J Phys Chem B 105: 2260–2263
[55] Bawendi MG, Carroll PJ, Wilson W, Brus L (1992) Luminescence properties of CdSe quantum crystallies: resonance between interior and surface localized states. J Chem Phys 96: 946–954
[56] Rakovich YP, Walsh L, Bradley L, Donegan JF, Talapin D, Rogach AL, Eychmüller A (2000) Size selective photoluminescence excitation spectroscopy in CdTe quantum dots. Proc SPIE 4876: 432–437
[57] Filonovich SA, Gomes MJM, Rakovich YP, Donegan JF, Talapin DV, Gaponik NP, Rogach AL, Eychmüller A (2003) Up-conversion luminescence in colloidal CdTe nanocrystals. MRS Proc 737: 157–162
[58] Vavilov S (1946) Photoluminescence and thermodynamics. J Phys 10: 499–502
[59] Rakovich YP, Donegan JF, Filonovich SA, Gomes MJM, Talapin DV, Rogach AL, Eychmüller A (2003) Up-conversion luminescence via a below-gap state in CdSe/ZnS quantum dots. Phys E 17: 99–100
[60] Carlone C, Beliveau A, Rowell NL (1991) On the anti-Stokes fluorescence in $Cd_{1-x}Zn_xS$ crystals. J Lumin 47: 309–317
[61] Joly AG, Chen W, McCready DE, Malm J-O, Bovin J-O (2005) Upconversion luminescence of CdTe nanoparticles. Phys Rev B 71: 165304–1/9
[62] Chen W (2005) Upconversion luminescence from CdSe nanoparticles. J Chem Phys 122: 224708–1/7
[63] Rakovich YP, Donegan JF, Filonovich SA, Gomes MJM, Talapin DV, Rogach AL, Eychmüller AA (2003) Photon energy up-conversion in CdSe quantum dots. In: Long AR, Davies JD (eds). Proceedings of the 26th International Conference on the Physics of Semiconductors. Edinburgh, UK: Institute of Physics Conference Series pp R2.7.1–R2.7
[64] Widulle F, Kramp S, Pyka NM, Gobel A, Ruf T, Debernardi A, Lauck R, Cardona M (1999) The phonon dispersion of wurtzite CdSe. Phys B 263–264: 4448–4451
[65] Vasilevskiy MI, Anda EV, Makler SS (2004) Electron–phonon interaction effects in semiconductor quantum dots: a nonperturabative approach. Phys Rev B 70: 035318–1/14
[66] Nirmal M, Murray CB, Bawendi MG (1994) Fluorescence-line narrowing in CdSe quantum dots: surface localization of the photogenerated exciton. Phys Rev B 50: 2293–2300
[67] Underwood DF, Kippeny T, Rosenthal SJ (2001) Ultrafast carrier dynamics in CdSe nanocrystals determined by femtosecond fluorescence upconversion spectroscopy. J Phys Chem B 105: 436–443
[68] Efros AL, Rosen M, Kuno M, Nirmal M, Norris DJ, Bawendi M (1996) Band-edge exciton in quantum dots of semiconductors with a degenerate valence band: dark and bright exciton states. Phys Rev B 54: 4843–4856
[69] Klimov VI, McBranch DW (1998) Femtosecond 1P-to-1S electron relaxation in strongly confined semiconductor nanocrystals. Phys Rev Lett 80: 4028–4031
[70] Baranov AV, Rakovich YP, Donegan JF, Perova TS, Moore RA, Talapin DV, Rogach AL, Masumoto Y, Nabiev I (2003) Effect of ZnS shell thickness on the phonon spectra in CdSe quantum dots. Phys Rev B 68: 165306–1/7
[71] Rakovich YP, Donegan JF, Gaponik N, Rogach AL (2003) Raman scattering and anti-Stokes emission from a single spherical microcavity with a CdTe quantum dot monolayer. Appl Phys Lett 83: 2539–2541
[72] Trallero-Giner C, Debernardi A, Cardona M, Menéndez-Proupín E, Ekimov AI (1998) Optical vibrons in CdSe dots and dispersion relation of the bulk material. Phys Rev B 57: 4664–4669
[73] Tamulaitis G, Rodrigues PAM, Yu PY (1995) Screening of longitudinal optical phonons by carriers in quantum dots. Sol Stat Commun 95: 227–231
[74] Rolo AG, Vasilevskiy MI, Gaponik NP, Rogach AL, Gomes MJM (2002) Confined optical vibrations in CdTe quantum dots and clusters. Phys Stat Sol (b) 229: 433–437
[75] Vasilevskiy MI (2002) Dipolar vibrational modes in spherical semiconductor quantum dots. Phys Rev B 66: 195326–1/9
[76] Hwang Y-N, Shin S, Park HL, Park S-H, Kim U, Jeong HS, Shin E-J, Kim D (1996) Effect of lattice ontraction on the Raman shifts of CdSe quantum dots in glass matrices. Phys Rev B 54: 15120–15124

[77] Hwang Y-N, Park S-H, Kim D (1999) Size-dependent surface phonon mode of CdSe quantum dots. Phys Rev B 59: 7285–7288
[78] Comas F, Trallero-Giner C, Studart N, Marques GE (2002) Interface optical phonons in spheroidal dots: Raman selection rules. Phys Rev B 65: 073303–1/3
[79] Rodriguez-Suarez R, Menendez-Proupin E, Trallero-Giner C, Cardona M (2000) Multiphonon resonant Raman scattering in nanocrystals. Phys Rev B 62: 11006–1/16
[80] Ruppin R, Englman R (1970) Optical phonons of small crystals. Rep Prog Phys 33: 146–196
[81] Fedorov AV, Baranov AV, Inoue K (1997) Exciton–phonon coupling in semiconductor quantum dots: resonant Raman scattering. Phys Rev B 56: 7491–7502
[82] Lee J, Govorov AO, Kotov NA (2005) Nanoparticle assemblies with molecular springs: a nanoscale thermometer. Angew Chem Int Ed 2005 44: 7439–7442
[83] Vahala KJ (2003) Optical microcavities. Nature 424: 839–846
[84] Braginsky VB, Gorodetsky ML, Ilchenko VS (1989) Quality factor and nonlinear properties of optical whispering-gallery modes. Phys Lett A 137: 393–397
[85] Hill SC, Benner RE (1986) Morphology-dependent resonances associated with stimulated processes in microspheres. J Opt Soc Am B 3: 1509–1514
[86] Gaponik N, Rakovich YP, Gerlach M, Donegan JF, Savateeva D, Rogach AL (2006) Whispering gallery modes in photoluminescence and Raman spectra of a spherical microcavity with CdTe quantum dots: anti-Stokes emission and interference effects. Nanoscale Res Lett 1: 68–73
[87] Pringsheim P (1929) Zwei Bemerkungen über den Unterschied von Lumineszenz- und Temperaturstrahlung. Z Physik 57: 739–746
[88] Epstein RI, Buchwald MI, Edwards BC, Gosnell TR, Mungan CE (1995) Observation of laser-induced fluorescent cooling of a solids. Nature 377: 500–503
[89] Clark JL, Rumbles G (1996) Laser cooling in the condensed phase by frequency up-conversion. Phys Rev Lett 76: 2037–2040
[90] Hoyt CW, Sheik-Bahae M, Epstein RI, Edwards BC, Anderson JE (2000) Observation of anti-Stokes fluorescence cooling in thulium-doped glass. Phys Rev Lett 87: 3600–3603
[91] Sheik-Bahae M, Epstein RI (2004) Can laser light cool semiconductors? Phys Rev Lett 92: 247403–1/4
[92] Alphandéry E, Walsh LM, Rakovich Y, Bradley AL, Donegan JF, Gaponik N (2004) Highly efficient Förster resonance energy transfer between CdTe nanocrystals and Rhodamine B in mixed solid films. Chem Phys Lett 388: 100–104
[93] Oraevsky AN (1996) Cooling of semiconductors by laser radiation. Quantum Electron 26: 1018–1022
[94] Rivlin LA, Zadernovsky AA (1997) Laser cooling of semiconductors. Opt Commun 139: 219–222
[95] Zander C, Drexhage KH (1995) Cooling of dye solution by anti-Stokes fluorescence. In: Neckers DC, Volman DH, von Bunau G (eds) Advances in photochemistry. Wiley, New York, pp 59–78